Mesolimbic dopamine ramps reflect environmental timescales

Joseph R Floeder[1], Huijeong Jeong[2], Ali Mohebi[2], and Vijay Mohan K Namboodiri[1,2,3,4]

[1]Neuroscience Graduate Program, University of California, San Francisco, CA, USA
[2]Department of Neurology, University of California, San Francisco, CA, USA
[3]Weill Institute for Neurosciences, Kavli Institute for Fundamental Neuroscience, Center for Integrative Neuroscience, University of California, San Francisco, CA, USA
[4]Correspondence to VijayMohan.KNamboodiri@ucsf.edu

Mesolimbic dopamine activity occasionally exhibits ramping dynamics, reigniting debate on theories of dopamine signaling. This debate is ongoing partly because the experimental conditions under which dopamine ramps emerge remain poorly understood. Here, we show that during Pavlovian and instrumental conditioning, mesolimbic dopamine ramps are only observed when the inter-trial interval is short relative to the trial period. These results constrain theories of dopamine signaling and identify a critical variable determining the emergence of dopamine ramps.

Mesolimbic dopamine activity was classically thought to operate in either a "phasic" or a "tonic" mode[1–3]. Yet, recent evidence points to a "quasi-phasic" mode in which mesolimbic dopamine activity exhibits ramping dynamics[4–16]. This discovery reignited debate on theories of dopamine function as it appeared inconsistent with the dominant theory that dopamine signaling conveys temporal difference reward prediction error (RPE)[17]. Recent work has hypothesized that dopamine ramps reflect the value of ongoing states[1, 4–6], RPE under some assumptions[8, 10, 18, 19], or a causal influence of actions on rewards in instrumental tasks[11]. This debate has been exacerbated in part because there is no clear understanding of why dopamine ramps appear only under some experimental conditions. Accordingly, uncovering a unifying principle of the conditions under which dopamine ramps appear will provide important constraints on theories of dopamine function[1, 11, 18, 20–39].

In our recent work proposing that dopamine acts as a teaching signal for causal learning by representing the Adjusted Net Contingency for Causal Relations (ANCCR)[20, 34, 40], simulated ANCCR depends on the duration of a memory trace of past events (i.e., on the "eligibility trace" time constant) (illustrated in Extended Data Fig 1). Accordingly, we successfully simulated dopamine ramping dynamics assuming two conditions: a dynamic progression of cues that signal temporal proximity to reward, and a small eligibility trace time constant relative to the trial period[20]. However, whether these conditions are sufficient to experimentally produce mesolimbic dopamine ramps in vivo remains untested. To test this prediction in Pavlovian conditioning, we measured mesolimbic dopamine release in the nucleus accumbens core using a dopamine sensor (dLight1.3b)[41] in an auditory cue-reward task. We varied both the presence or absence of a progression of cues indicating reward proximity ("dynamic" vs "fixed" tone) and the inter-trial interval (ITI) duration (short vs long ITI). Varying the ITI was critical because our theory predicts that the ITI is a variable controlling the eligibility trace time constant, such that a short ITI would produce a small time constant relative to the cue-reward interval (Supplementary Note 1) (Fig 1a-e). In all four task conditions, head-fixed mice learned to anticipate the sucrose reward, as reflected by anticipatory licking (Fig 1f-g). In line with our earlier work, we showed that simulations of ANCCR exhibit a larger cue onset response when the ITI is long and exhibit ramps only when the ITI is short (Fig 1h). Consistent with these simulated predictions, experimentally measured mesolimbic dopamine release had a much higher cue onset response for long ITI (Fig 1i-j). Furthermore, dopamine ramps were observed only when the ITI was short and the tone was dynamic (Fig 1i, k-m). The presence of dopamine ramps during the last five seconds of the cue could not be explained by variations in behavior, as anticipatory licking during this period was similar across all conditions (Extended Data Fig 2, Supplementary Note 2). Indeed, dopamine ramps—quantified by a positive slope of dopamine response vs time within trial over the last five seconds of the cue—appeared on the first day after transition from a long ITI/dynamic tone condition to a short ITI/dynamic tone condition and disappeared on the first day after transition from a short ITI/dynamic tone condition to a short ITI/fixed tone condition (Fig 1l). These results confirm the key prediction of our theory in Pavlovian conditioning.

Given the speed with which dopamine ramps appeared and disappeared, we next tested whether the slope of dopamine ramps in the short ITI/dynamic tone condition depended on the previous ITI duration on a trial-by-trial basis. We found that there was indeed a statistically significant trial-by-trial correlation between the previous ITI duration and the current trial's dopamine response slope in the short ITI/dynamic condition with ramps, but not in the long ITI/dynamic condition without ramps (Fig 2, Extended Data Fig 3). The dependence of a trial's dopamine response slope with previous ITI was significantly negative, meaning that a longer ITI correlates with a weaker ramp on the next trial. This finding held when analyzing either animal-by-animal (Fig 2a-b) or the pooled trials across animals while accounting for mean animal-by-animal variability (Fig 2c). These results suggest that the eligibility trace time constant adapts rapidly to changing ITI in Pavlovian conditioning.

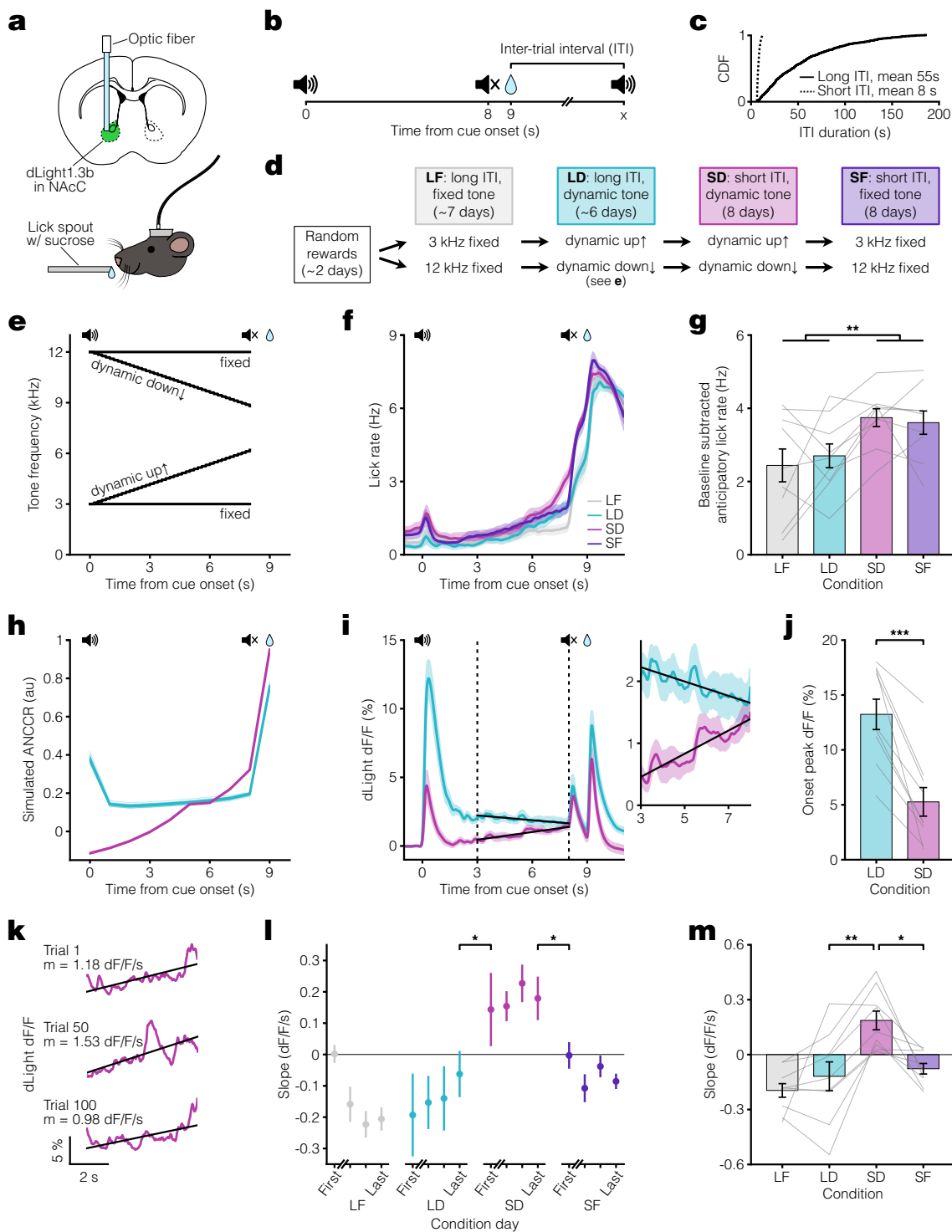We next tested whether the results from Pavlovian

Fig. 1. Pavlovian conditioning dopamine ramps depend on ITI. a. Top, fiber photometry approach schematic for nucleus accumbens core (NAcC) dLight recordings. Bottom, head-fixed mouse. **b**. Pavlovian conditioning task setup. Trials consisted of an 8 s auditory cue followed by sucrose reward delivery 1 s later. **c**. Cumulative Distribution Function (CDF) of ITI duration for long (solid line, mean 55 s) and short ITI (dashed line, mean 8 s) conditions. **d**. Experimental timeline. Mice were divided into groups receiving either a 3 kHz fixed and dynamic up↑ tone or a 12 kHz fixed and dynamic down↓ tone. **e**. Tone frequency over time. **f**. Peri-stimulus time histogram (PSTH) showing average licking behaviors for the last 3 days of each condition (n = 9 mice). **g**. Average anticipatory lick rate (baseline subtracted) for 1 s preceding reward delivery (two-way ANOVA: long ITI vs short ITI $F_{(1)}$ = 9.3, **p = 0.0045). **h**. ANCCR simulation results from an 8 s dynamic cue followed by reward 1 s later for long ITI (teal) and short ITI (pink) conditions. Bold lines show the average of 20 iterations. **i**. Left, average dLight dopamine signals. Vertical dashed lines represent the ramp window from 3 to 8 s after cue onset, thereby excluding the influence of the cue onset and offset responses. Solid black lines show linear regression fit during window. Right, closeup of dopamine signal during window. **j**. Average peak dLight response to cue onset for LD and SD conditions (paired t-test: t(8) = 6.3, ***p = 2.3×10⁻⁴). **k**. dLight dopamine signal with linear regression fit during ramp window for example SD trials. Reported m is slope. **l**. Session average per-trial slope during ramp window for the first day and last 3 days of each condition (one-sided [last day LD < first day SD] paired t-test: t(8) = -2.1, *p = 0.036; one-sided [last day SD > first day SF] paired t-test: t(8) = 2.4, *p = 0.023). **m**. Average per-trial slope for last 3 days of each condition (Tukey HSD test: q = 3.8, LD vs SD **p = 0.0027, SD vs SF *p = 0.011). All data presented as mean ± SEM. See Supplementary Table 1 for full statistical details.
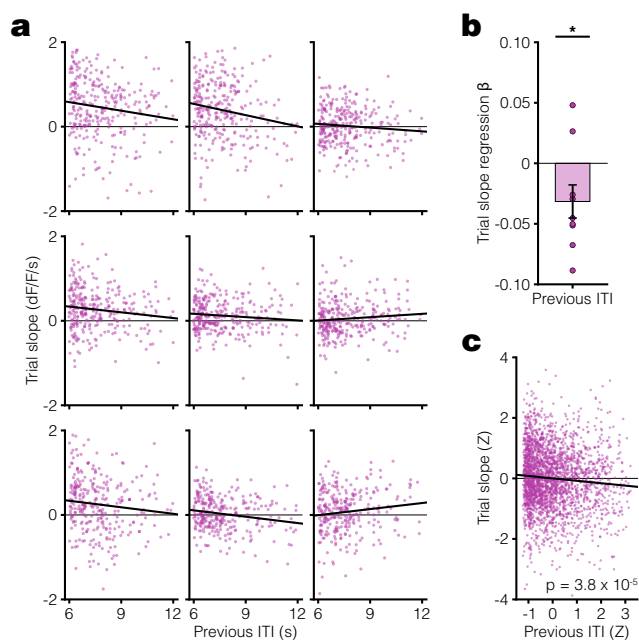
Fig. 2. Per-trial dopamine ramps correlate with previous ITI. a. Scatter plots showing the relationship between dopamine response slope within a trial and previous ITI for all trials in the last 3 days of SD condition. Each animal plotted individually with linear regression fit (black line). **b**. Linear regression β coefficients for previous ITI vs. trial slope calculated per animal (one-sided [< 0] one sample t-test: t(8) = -2.2, *p = 0.031). **c**. Scatter plot of Z-scored trial slope vs. previous ITI pooled across mice for all trials in the last 3 days of LD condition (linear regression: t(2671) = -4.1, R^2 = 0.0063, ***p = 3.8 $\times 10^{-5}$). The Z-scoring per animal removes the effect of variable means across animals on the slope of the pooled data. All data presented as mean ± SEM. See Supplementary Table 1 for full statistical details.

conditioning could be reproduced in an instrumental task. In keeping with prior demonstrations of dopamine ramps in head-fixed mice, we used a virtual reality (VR) navigational task in which head-fixed mice had to run towards a destination in a virtual hallway to obtain sucrose rewards (8, 10, 18, 42) (Fig 3a-b, Extended Data Fig 4). At reward delivery, the screen turned blank during the ITI and remained so until the next trial onset. After training animals in this task using a medium ITI, we changed the ITI duration to short or long for eight days before switching to the other (Fig 3c). We found evidence that mice learned the behavioral requirement during the trial period, as they significantly increased their running speed during trial onset (Fig 3d-e) and reached a similarly high speed prior to reward in both ITI conditions (Fig 3f-g). Consistent with the results from Pavlovian conditioning, the dopamine response to the onset of the hallway presentation was larger during the long ITI compared to the short ITI condition (Fig 3h-i), and dopamine ramps were observed only in the short ITI condition (Fig 3j-m). Unlike the Pavlovian conditioning, the change in the ITI resulted in a more gradual appearance or disappearance of ramps (Fig 3k), but there was still a weak overall correlation between dopamine response slope on a trial and the previous inter-reward interval (Extended Data Fig 5). These results are consistent with a more gradual change in the eligibility trace time constant in this instrumental task. Collectively, the core finding from Pavlovian conditioning that mesolimbic dopamine ramps are present only during short ITI conditions was reproduced in the instrumental VR task.

Our results provide a general framework for understanding past results on dopamine ramps. According to ANCCR, the fundamental variable controlling the presence of ramps is the eligibility trace time constant. Based on first principles, this time constant depends on the ITI in common task designs (Supplementary Note 1). Thus, the ITI is a simple proxy to manipulate the eligibility trace time constant, thereby modifying dopamine ramps. In previous navigational tasks with dopamine ramps, there was no explicitly programmed ITI (4, 7, 13). As such, the controlling of the pace of trials by these highly motivated animals likely resulted in short effective ITI compared to trial duration. An instrumental lever pressing task with dopamine ramps similarly had no explicitly programmed ITI(9), and other tasks with observed ramps had short ITIs(8, 10, 12, 15, 16). One reported result that does not fit with a simple control of ramps by ITI is that navigational tasks produce weaker ramps with repeated training(7). These results are generally inconsistent with the stable ramps that we observed in Pavlovian conditioning across eight days (Fig 1l). A speculative explanation might be that when the timescales of events vary considerably (e.g., during early experience in instrumental tasks due to variability in action timing), animals use a short eligibility trace time constant to account for the potential non-stationarity of the environment. With repeated exposure, the experienced stationarity of the environment might increase the eligibility trace time constant, thereby complicating its relationship with the ITI. Alternatively, as suggested previously(7), repeated navigation may result in automated behavior that ignores the progress towards reward, thereby minimizing the calculation of associations of spatial locations with reward. Another set of observations superficially inconsistent with our assumption of the necessity of a sequence of external cues signaling proximity to reward for ramping to occur is that dopamine ramping dynamics can be observed even when only internal states signal reward proximity (e.g., timing a delayed action) (7, 12, 15). In these cases, however, animals were required to actively keep track of the passage of time, which therefore strengthens an internal progression of neural states signaling temporal proximity to reward. Once learned, these internal states could serve the role of external cues in the ANCCR framework (Supplementary Note 3).

Though the current experiments in this study were motivated by the ANCCR framework, they were not conducted to discriminate between theories. As such, though the data are largely consistent with ANCCR, they should not be treated as evidence explicitly for ANCCR (Supplementary Note 4). It may also be possible that these results can be explained by other theories of dopamine function. For instance, temporal discounting may depend on overall reward rate(23, 43, 44), and such changes in temporal discounting may affect predictions in alternative theories such as temporal difference value or RPE dopamine signaling. Regardless of such considerations, the current results provide a clear constraint for dopamine theories and demonstrate that an underappreciated experimental variable determines the emergence of mesolimbic dopamine ramps.
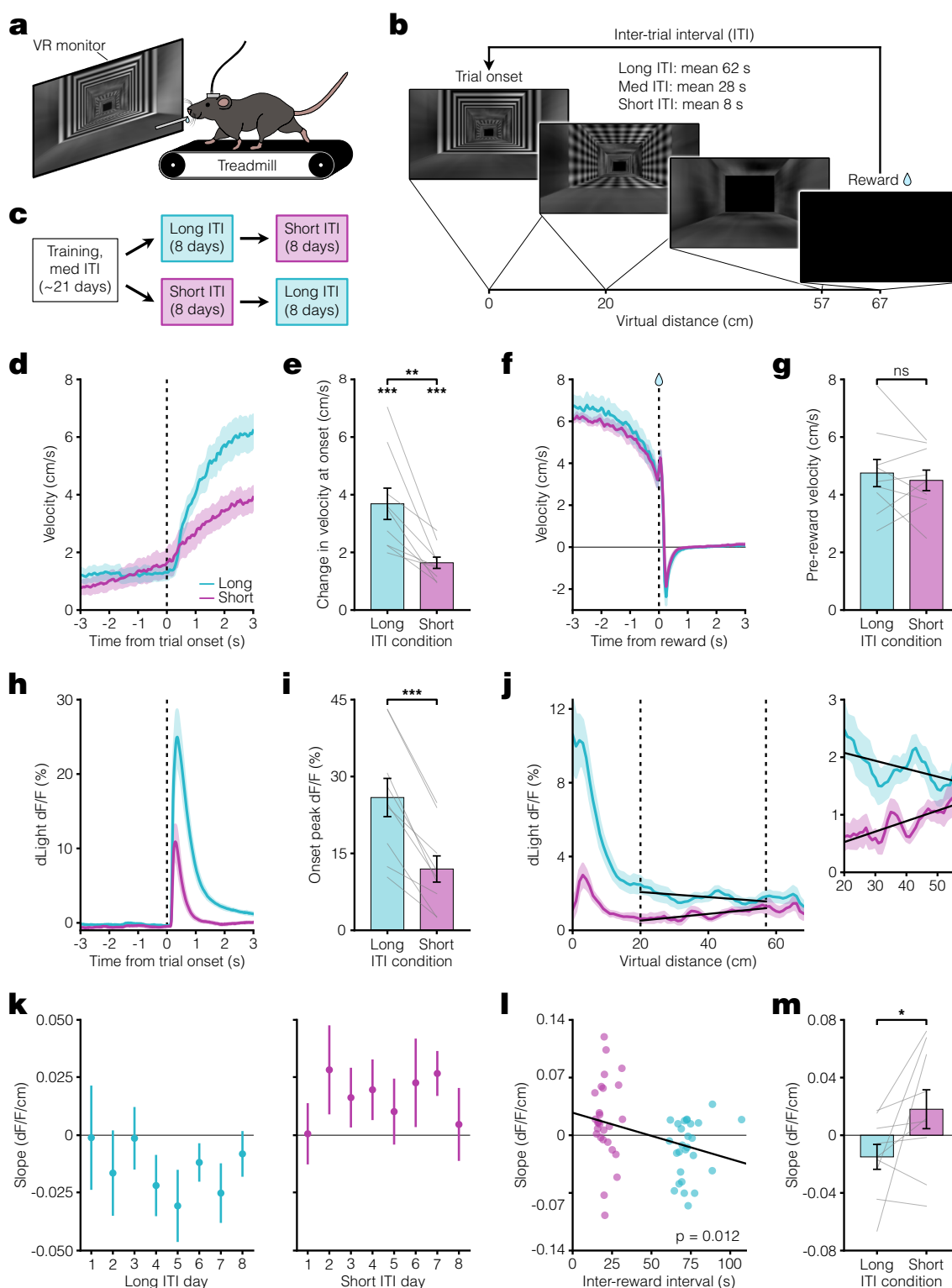
Fig. 3. VR navigation dopamine ramps depend on ITI. a. Head-fixed VR approach schematic. **b**. VR navigation task setup. Trials consisted of running down a patterned virtual hallway to receive sucrose reward. VR monitor remained black during the ITI. **c**. Experimental timeline. Following training, mice were assigned to either long or short ITI conditions for 8 days before switching. **d**. Velocity PSTH aligned to trial onset for long (teal) and short (pink) ITI conditions (n = 9 mice). **e**. Average change in velocity at trial onset. Bottom asterisks indicate both conditions significantly differ from zero (one-sided [> 0] one sample t-test: long ITI t(8) = 6.4, ***p = 1.0×10^{-4}; short ITI t(8) = 7.9, ***p = 2.3×10^{-5}). Top asterisks indicate significant difference between conditions (paired t-test: t(8) = 4.3, **p = 0.0028. **f**. Velocity PSTH aligned to reward delivery. **g**. Average velocity during 1 s preceding reward (paired t-test: t(8) = 0.71, p = 0.50). **h**. PSTH showing average dLight dopamine signal aligned to trial onset. **i**. Comparison of peak dLight onset response (paired t-test: t(8) = 7.6, ***p = 6.3×10^{-5}). **j**. Left, average dLight dopamine signal across distances spanning the entire virtual corridor. Vertical dashed lines represent the ramp window from 20 to 57 cm (10 cm before end of track). Solid black lines show linear regression fit during window. Right, closeup of dopamine signal during window. **k**. Session average per-trial slope during ramp window for all days of each condition. **l**. Scatter plot showing relationship between average per-session slope and inter-reward interval for the last 3 days in long (teal) and short (pink) ITI conditions. Black line indicates linear regression fit (linear regression: t(53) = -2.6, R^2 = 0.12, *p = 0.012). **m**. Comparison of average per-trial slope during ramp window for last 3 days of both conditions (one-sided [long < short] paired t-test: t(8) = -2.1, *p = 0.035). All data presented as mean ± SEM. See Supplementary Table 1 for full statistical details.

AUTHOR CONTRIBUTIONS

J.R.F. and V.M.K.N. conceived the project. J.R.F. performed experiments and analyses. H.J. performed simulations. A.M. helped with the design and instrumentation of the VR experiment. V.M.K.N. oversaw all aspects of the study. J.R.F. and V.M.K.N. wrote the manuscript with help from all authors.

Bibliography

1. Joshua D Berke. What does dopamine mean? *Nature Neuroscience*, 21(6):787–793, 2018.

2. Anthony A Grace. Phasic versus tonic dopamine release and the modulation of dopamine system responsivity: a hypothesis for the etiology of schizophrenia. *Neuroscience*, 41(1):1–24, 1991.

3. Yael Niv, Nathaniel D Daw, Daphna Joel, and Peter Dayan. Tonic dopamine: opportunity costs and the control of response vigor. *Psychopharmacology*, 191:507–520, 2007.

4. Mark W Howe, Patrick L Tierney, Stefan G Sandberg, Paul EM Phillips, and Ann M Graybiel. Prolonged dopamine signalling in striatum signals proximity and value of distant rewards. *Nature*, 500(7464):575–579, 2013.

5. Arif A Hamid, Jeffrey R Pettibone, Omar S Mabrouk, Vaughn L Hetrick, Robert Schmidt, Caitlin M Vander Weele, Robert T Kennedy, Brandon J Aragona, and Joshua D Berke. Mesolimbic dopamine signals the value of work. *Nature Neuroscience*, 19(1):117–126, 2016.

6. Ali Mohebi, Jeffrey R Pettibone, Arif A Hamid, Jenny-Marie T Wong, Leah T Vinson, Tommaso Patriarchi, Lin Tian, Robert T Kennedy, and Joshua D Berke. Dissociable dopamine dynamics for learning and motivation. *Nature*, 570(7759):65–70, 2019.

7. Akash Guru, Changwoo Seo, Ryan J Post, Durga S Kullakanda, Julia A Schaffer, and Melissa R Warden. Ramping activity in midbrain dopamine neurons signifies the use of a cognitive map. *bioRxiv*, pages 2020–05, 2020.

8. HyungGoo R Kim, Athar N Malik, John G Mikhael, Pol Bech, Iku Tsutsui-Kimura, Fangmiao Sun, Yajun Zhang, Yulong Li, Mitsuko Watabe-Uchida, Samuel J Gershman, et al. A unified framework for dopamine signals across timescales. *Cell*, 183(6):1600–1616, 2020.

9. Anne L Collins, Venuz Y Greenfield, Jeffrey K Bye, Kay E Linker, Alice S Wang, and Kate M Wassum. Dynamic mesolimbic dopamine signaling during action sequence learning and expectation violation. *Scientific Reports*, 6(1):20231, 2016.

10. Karolina Farrell, Armin Lak, and Aman B Saleem. Midbrain dopamine neurons signal phasic and ramping reward prediction error during goal-directed navigation. *Cell Reports*, 41(2), 2022.

11. Arif A Hamid, Michael J Frank, and Christopher I Moore. Wave-like dopamine dynamics as a mechanism for spatiotemporal credit assignment. *Cell*, 184(10):2733–2749, 2021.

12. Allison E Hamilos, Giulia Spedicato, Ye Hong, Fangmiao Sun, Yulong Li, and John A Assad. Slowly evolving dopaminergic activity modulates the moment-to-moment probability of reward-related self-timed movements. *eLife*, 10:e62583, 2021.

13. Timothy A Krausz, Alison E Comrie, Ari E Kahn, Loren M Frank, Nathaniel D Daw, and Joshua D Berke. Dual credit assignment processes underlie dopamine signals in a complex spatial environment. *Neuron*, 111(21):3465–3478, 2023.

14. Ben Engelhard, Joel Finkelstein, Julia Cox, Weston Fleming, Hee Jae Jang, Sharon Ornelas, Sue Ann Koay, Stephan Y Thiberge, Nathaniel D Daw, David W Tank, et al. Specialized coding of sensory, motor and cognitive variables in vta dopamine neurons. *Nature*, 570(7762):509–513, 2019.

15. Zilong Gao, Hanqing Wang, Chen Lu, Tiezhan Lu, Sean Froudist-Walsh, Ming Chen, Xiao-Jing Wang, Ji Hu, and Wenzhi Sun. The neural basis of delayed gratification. *Science Advances*, 7(49):eabg6611, 2021.

16. Emilie CJ Syed, Laura L Grima, Peter J Magill, Rafal Bogacz, Peter Brown, and Mark E Walton. Action initiation shapes mesolimbic dopamine encoding of future rewards. *Nature Neuroscience*, 19(1):34–36, 2016.

17. Yael Niv. Dopamine ramps up. *Nature*, 500(7464):533–535, 2013.

18. John G Mikhael, HyungGoo R Kim, Naoshige Uchida, and Samuel J Gershman. The role of state uncertainty in the dynamics of dopamine. *Current Biology*, 32(5):1077–1087, 2022.

19. Kenji Morita and Ayaka Kato. A neural circuit mechanism for the involvements of dopamine in effort-related choices: decay of learned values, secondary effects of depletion, and calculation of temporal difference error. *eNeuro*, 5(1), 2018.

20. Huijeong Jeong, Annie Taylor, Joseph R Floeder, Martin Lohmann, Stefan Mihalas, Brenda Wu, Mingkang Zhou, Dennis A Burke, and Vijay Mohan K Namboodiri. Mesolimbic dopamine release conveys causal associations. *Science*, 378(6626):eabq6740, 2022.

21. Luke T Coddington, Sarah E Lindo, and Joshua T Dudman. Mesolimbic dopamine adapts the rate of learning from action. *Nature*, 614(7947):294–302, 2023.

22. Munir Gunes Kutlu, Jennifer E Zachry, Patrick R Melugin, Stephanie A Cajigas, Maxime F Chevee, Shannon J Kelly, Banu Kutlu, Lin Tian, Cody A Siciliano, and Erin S Calipari. Dopamine release in the nucleus accumbens core signals perceived saliency. *Current Biology*, 31(21):4748–4761, 2021.

23. Margarida Sousa, Pawel Bujalski, Bruno F Cruz, Kenway Louie, Daniel McNamee, and Joseph J Paton. Dopamine neurons encode a multidimensional probabilistic map of future reward. *bioRxiv*, pages 2023–11, 2023.

24. Matthew PH Gardner, Geoffrey Schoenbaum, and Samuel J Gershman. Rethinking dopamine as generalized prediction error. *Proceedings of the Royal Society B*, 285(1891):20181645, 2018.

25. Melissa J Sharpe, Hannah M Batchelor, Lauren E Mueller, Chun Yun Chang, Etienne JP Maes, Yael Niv, and Geoffrey Schoenbaum. Dopamine transients do not act as model-free prediction errors during associative learning. *Nature Communications*, 11(1):106, 2020.

26. Francis Carter, Marie-Pierre Cossette, Ivan Trujillo-Pisanty, Vasilios Pallikaras, Yannick-André Breton, Kent Conover, Jill Caplan, Pavel Solis, Jacques Voisard, Alexandra Yaksich, et al. Does phasic dopamine release cause policy updates? *European Journal of Neuroscience*, 2023.

27. Ryan N Hughes, Konstantin I Bakhurin, Elijah A Petter, Glenn DR Watson, Namsoo Kim, Alexander D Friedman, and Henry H Yin. Ventral tegmental dopamine neurons control the impulse vector during motivated behavior. *Current Biology*, 30(14):2681–2694, 2020.

28. Scott Waddell. Reinforcement signalling in drosophila; dopamine does it all after all. *Current Opinion in Neurobiology*, 23(3):324–329, 2013.

29. Jeffrey E Markowitz, Winthrop F Gillis, Maya Jay, Jeffrey Wood, Ryley W Harris, Robert Cieszkowski, Rebecca Scott, David Brann, Dorothy Koveal, Tomasz Kula, et al. Spontaneous behaviour is structured by reinforcement without explicit reward. *Nature*, 614(7946):108–117, 2023.

30. Jonathan CY Tang, Vitor Paixao, Filipe Carvalho, Artur Silva, Andreas Klaus, Joaquim Alves da Silva, and Rui M Costa. Dynamic behaviour restructuring mediates dopamine-dependent credit assignment. *Nature*, 626(7999):583–592, 2024.

31. Kent C Berridge. The debate over dopamine's role in reward: the case for incentive salience. *Psychopharmacology*, 191:391–431, 2007.

32. Ana C Sias, Yousif Jafar, Caitlin M Goodpaster, Kathia Ramírez-Armenta, Tyler M Wrenn, Nicholas K Griffin, Keshav Patel, Alexander C Lamparelli, Melissa J Sharpe, and Kate M Wassum. Dopamine projections to the basolateral amygdala drive the encoding of identity-specific reward memories. *Nature Neuroscience*, pages 1–9, 2024.

33. Etienne J P Maes, Melissa J Sharpe, Alexandra A Usypchuk, Megan Lozzi, Chun Yun Chang, Matthew PH Gardner, Geoffrey Schoenbaum, and Mihaela D Iordanova. Causal evidence supporting the proposal that dopamine transients function as temporal difference prediction errors. *Nature Neuroscience*, 23(2):176–178, 2020.

34. Eric Garr, Yifeng Cheng, Huijeong Jeong, Sara Brooke, Laia Castell, Aneesh Bal, Robin Magnard, Vijay Mohan K Namboodiri, and Patricia H Janak. Mesostriatal dopamine is sensitive to specific cue-reward contingencies. *bioRxiv*, pages 2023–06, 2023.

35. Anthony Jakob, John G Mikhael, Allison E Hamilos, John A Assad, and Samuel J Gershman. Dopamine mediates the bidirectional update of interval timing. *Behavioral Neuroscience*, 136(5):445, 2022.

36. Benjamin T Saunders, Jocelyn M Richard, Elyssa B Margolis, and Patricia H Janak. Dopamine neurons create pavlovian conditioned stimuli with circuit-defined motivational properties. *Nature Neuroscience*, 21(8):1072–1083, 2018.

37. Yuji K Takahashi, Thomas A Stalnaker, Lauren E Mueller, Sevan K Harootonian, Angela J Langdon, and Geoffrey Schoenbaum. Dopaminergic prediction errors in the ventral tegmental area reflect a multithreaded predictive model. *Nature Neuroscience*, 26(5):830–839, 2023.

38. Peter Redgrave and Kevin Gurney. The short-latency dopamine signal: a role in discovering novel actions? *Nature Reviews Neuroscience*, 7(12):967–975, 2006.

39. Ethan S Bromberg-Martin, Masayuki Matsumoto, and Okihide Hikosaka. Dopamine in motivational control: rewarding, aversive, and alerting. *Neuron*, 68(5):815–834, 2010.

40. Dennis A Burke, Huijeong Jeong, Brenda Wu, Seul Ah Lee, Joseph R Floeder, and Vijay Mohan K Namboodiri. Few-shot learning: temporal scaling in behavioral and dopaminergic learning. *bioRxiv*, 2023.

41. Tommaso Patriarchi, Jounhong Ryan Cho, Katharina Merten, Mark W Howe, Aaron Marley, Wei-Hong Xiong, Robert W Folk, Gerard Joey Broussard, Ruqiang Liang, Min Jee Jang, et al. Ultrafast neuronal imaging of dopamine dynamics with designed genetically encoded sensors. *Science*, 360(6396):eaat4422, 2018.

42. Gonçalo Lopes, Karolina Farrell, Edward AB Horrocks, Chi-Yu Lee, Mai M Morimoto, Tomaso Muzzu, Amalia Papanikolaou, Fabio R Rodrigues, Thomas Wheatcroft, Stefano Zucca, et al. Creating and controlling visual environments using bonvision. *eLife*, 10:e65541, 2021.

43. Vijay Mohan K Namboodiri, Stefan Mihalas, and Marshall GH Shuler. Rationalizing decision-making: understanding the cost and perception of time. *Timing & Time Perception Reviews*, 1, 2014.

44. Douglas A Williams, Travis P Todd, Chrissy M Chubala, and Elliot A Ludvig. Intertrial unconditioned stimuli differentially impact trace conditioning. *Learning & Behavior*, 45:49–61, 2017.

45. Mingkang Zhou, Brenda Wu, Huijeong Jeong, Dennis A Burke, and Vijay Mohan K Namboodiri. An open-source behavior controller for associative learning and memory (b-calm). *Behavior Research Methods*, pages 1–16, 2023.

46. Vijay Mohan K Namboodiri. How do real animals account for the passage of time during associative learning? *Behavioral Neuroscience*, 136(5):383, 2022.

Methods

Animals. All experimental procedures were approved by the Institutional Animal Care and Use Committee at UCSF and followed guidelines provided by the NIH Guide for the Care and Use of Laboratory Animals. A total of eighteen adult wild-type C57BL/6J mice (000664, Jackson Laboratory) were divided between experiments: nine mice (4 females, 5 males) were used for Pavlovian conditioning, and nine mice (6 females, 3 males) were used for the VR task. Following surgery, mice were single housed in a reverse 12-hour light/dark cycle. Mice received environmental enrichment and had ad libitum access to standard chow. To increase motivation, mice underwent water deprivation. During deprivation, mice were weighed daily and given enough fluids to maintain 85% of their baseline weight.

Surgeries. Surgical procedures were always done under aseptic conditions. Induction of anesthesia was achieved with 3% isoflurane, which was maintained at 1-2% throughout the duration of the surgery. Mice received subcutaneous injections of carprofen (5 mg/kg) for analgesia and lidocaine (1 mg/kg) for local anesthesia of the scalp prior to incision. A unilateral injection (Nanoject III, Drummond) of 500 nL of dLight1.3b (AAVDJ-CAG-dLight1.3b, 2.4×10^{13} GC/mL diluted 1:10 in sterile saline) was targeted to the NAcC using the following coordinates from bregma: AP 1.3, ML $\pm$1.4, DV -4.55. The glass injection pipette was held in place for 10 minutes prior to removal to prevent the backflow of virus. After viral injection, an optic fiber (NA 0.66, 400 µm, Doric Lenses) was implanted 100 µm above the site of injection. Subsequently, a custom head ring for head-fixation was secured to the skull using screws and dental cement. Mice recovered and were given at least three weeks before starting behavioral experiments. After completion of experiments, mice underwent transcardial perfusion and subsequent brain fixation in 4% paraformaldehyde. Fiber placement was verified using 50 µm brain sections under a Keyence microscope.

Behavioral Tasks. All behavioral tasks took place during the dark cycle in dark, soundproof boxes with white noise playing to minimize any external noise. Prior to starting the Pavlovian conditioning task, water-deprived mice underwent 1-2 days of random rewards training to get acclimated to our head-fixed behavior setup(45). In a training session, mice received 100 sucrose rewards (3 µL, 15% in water) at random time intervals taken from an exponential distribution averaging 12 s. Mice consumed sucrose rewards from a lick spout positioned directly in front of their mouths. This same spout was used for lick detection. After completing random rewards, mice were trained on the Pavlovian conditioning task. An identical trial structure was used across all conditions of the task, consisting of an auditory tone lasting 8 s followed by a delay of 1 s before sucrose reward delivery. Two variables of interest were manipulated—the length of the ITI (long or short) and the type of auditory tone (fixed or dynamic)—resulting in four conditions: long ITI/fixed tone (LF), long ITI/dynamic tone (LD), short ITI/dynamic tone (SD), and short ITI/fixed tone (SF). Mice began with the LF condition (mean 7.4 days, range 7-8) before progressing to the LD condition (mean 6.1 days, range 5-11), the SD condition (8 days), and finally the SF condition (8 days). The ITI was defined as the period between reward delivery and the subsequent trial's cue onset. In the long ITI conditions, the ITI was drawn from a truncated exponential distribution with a mean of 55 s, maximum of 186 s, and minimum of 6 s. The short ITIs were similarly drawn from a truncated exponential distribution, averaging 8 s with a maximum of 12 s and minimum of 6 s. While mice had 100 trials per day in the short ITI conditions, long ITI sessions were capped at 40 trials due to limitations on the amount of time animals could spend in the head-fixed setup. For the fixed tone conditions, mice were randomly divided into groups presented with either a 3 kHz or 12 kHz tone. While the 12 kHz tone played continuously throughout the entire 8 s, the 3 kHz tone was pulsed (200 ms on, 200 ms off) to make this lower frequency tone more obvious to the mice. For the dynamic tone conditions, the tone frequency either increased (dynamic up↑ starting at 3 kHz) or decreased (dynamic down↓ starting at 12 kHz) by 80 Hz every 200ms, for a total change of 3.2 kHz across 8 s. Mice with the 3 kHz fixed tone had the dynamic up↑ tone, whereas mice with the 12 kHz fixed tone had the dynamic down↓ tone. This dynamic change in frequency across the 8 s was intentionally designed to indicate to the mice the temporal proximity to reward, which is thought to be necessary for ramps to appear in a Pavlovian setting.

For the VR task, water-deprived mice were head fixed above a low-friction belt treadmill46. A magnetic rotary encoder attached to the treadmill was used to measure the running velocity of the mice. In front of the head-fixed treadmill setup, a virtual environment was displayed on a high-resolution monitor (20" screen, 16:9 aspect ratio) to look like a dead-end hallway with a patterned floor, walls, and ceiling. The different texture patterns in the virtual environment were yoked to running velocity such that it appeared as though the animal was travelling down the hallway. Upon reaching the end of the hallway, the screen would turn fully black and mice would receive sucrose reward delivery from a lick spout positioned within reach in front of them. The screen remained black for the full duration of the ITI until the reappearance of the starting frame of the virtual hallway signaled the next trial onset. To train mice to engage in this VR task, they began with a 10 cm long virtual hallway. This minimal distance requirement was chosen to make it relatively easy for the mice to build associations between their movement on the treadmill, the corresponding visual pattern movement displayed on the VR monitor, and reward deliveries. Based on their performance throughout training, the distance requirement progressively increased by increments of 5-20 cm across days until reaching a maximum distance of 67 cm. Training lasted an average of 21.4 days (range 11-38 days), ending once mice could consistently run down the full 67 cm virtual hallway for three consecutive days. The ITIs during training ("med ITI") were randomly drawn from a truncated exponential distribution with a mean of 28 s, maximum of 90 s, and minimum of 6 s. Following training, mice were randomly divided into two groups with identical trials but different ITIs (long or short). Again, both ITIs were randomly

Floeder, Jeong, Mohebi, Namboodiri | Mesolimbic dopamine ramps reflect environmental timescales

drawn from truncated exponential distributions: long ITI (mean 62 s, max 186 s, min 6 s) and short ITI (mean 8 s, max 12 s, min 6 s). After 8 days of the first ITI condition, mice switched to the other condition for an additional 8 days. There were 50 trials per day in both the long and short ITI conditions.

Fiber Photometry. Beginning three weeks after viral injection, dLight photometry recordings were performed with either an open-source (PyPhotometry) or commercial (Doric Lenses) fiber photometry system. Excitation LED light for wavelengths of 470 nm (dopamine dependent dLight signal) and 405 nm (dopamine independent isosbestic signal) were sinusoidally modulated via an LED driver and integrated into a fluorescence minicube (Doric Lenses). The same minicube was used to detect incoming fluorescent signals at a 12 kHz sampling frequency before demodulation and downsampling to 120 Hz. Excitation and emission light passed through the same low autofluorescence patchcord (400 µm, 0.57 NA, Doric Lenses). Light intensity at the tip of this patchcord was consistently 40 µW across days. For Pavlovian conditioning, the photometry software received a TTL signal for the start and stop of the session to align the behavioral and photometry data. For alignment in the VR task, the photometry software received a TTL signal at each reward delivery.

Data Analysis. Behavior: Licking was the behavioral readout of learning used in Pavlovian conditioning. The lick rate was calculated by binning the number of licks every 100 ms. A smoothed version produced by Gaussian filtering is used to visualize lick rate in PSTHs (Fig 1f, Ext Data Fig 4d). Anticipatory lick rate for the last three days combined per condition was calculated by subtracting the average baseline lick rate during the 1 s before cue onset from the average lick rate during the trace period 1 s before reward delivery (Fig 1g). The same baseline subtraction method was used to calculate the average lick rate during the 3 to 8 s post cue onset period (Ext Data Fig 2d).

Running velocity, rather than licking, was the primary behavioral readout of learning for the VR task. Velocity was calculated as the change in distance per time. Distance measurements were sampled every 50 ms throughout both the trial and ITI periods. Average PSTHs from the last three days per condition were used to visualize velocity aligned to trial onset (Fig 3d) and reward delivery (Fig 3f). The change in velocity at trial onset was calculated by subtracting the average baseline velocity (baseline being 1 s before trial onset) from the average velocity between 1-2 s after trial onset (Fig 3e). Pre-reward velocity was the mean velocity during the 1 s period before reward delivery (Fig 3g). In addition to analyzing velocity, the average lick rate for the 1 s before reward delivery was used to quantify the modest anticipatory lick rate in the VR task (Ext Data Fig 4e). The inter-trial interval (ITI) used throughout is defined as the time period between the previous trial reward delivery and the current trial onset (Fig 1c, Fig 2a, Ext Data Fig 3, Ext Data Fig 4b). The inter-reward interval (IRI) is defined as the time period between the previous trial reward delivery and the current trial reward delivery (Fig 3l, Ext Data Fig 4b, Ext Data Fig 5). For the previous IRI vs trial slope analysis (Ext Data Fig 5), IRI outliers were removed from analysis if they were more than three standard deviations away from the mean of the original IRI distribution. Finally, trial durations in the VR task were defined as the time it took for mice to run 67 cm from the start to the end of the virtual hallway (Ext Data Fig 4b-c).

Dopamine: To analyze dLight fiber photometry data, first a least-square fit was used to scale the 405 nm signal to the 470 nm signal. Then, a percentage dF/F was calculated as follows: dF/F = (470 – fitted 405) / (fitted 405) * 100. This session-wide dF/F was then used for subsequent analysis. The onset peak dF/F (Figs 1j, 3i) was calculated by finding the maximum dF/F value within 1 s after onset and then subtracting the average dF/F value during the 1 s interval preceding onset (last three days per condition combined). For each trial in Pavlovian conditioning, the time aligned dLight dF/F signal during the "ramp window" of 3 to 8 s after cue onset was fit with linear regression to obtain a per-trial slope. These per-trial slopes were then averaged for each day separately (Fig 1l) or for the last three days in each condition (Fig 1m) for subsequent statistical analysis. A smoothing Gaussian filter was applied to the group average (Fig 1i) and example trial (Fig 1k) dLight traces for visualization purposes. Distance, rather than time, was used to align the dLight dF/F signal in the VR task. Virtual distances were sampled every 30 ms, while dF/F values were sampled every 10 ms. To sync these signals, the average of every three dF/F values was assigned to the corresponding distance value. Any distance value that did not differ from the previous distance value was dropped from subsequent analysis (as was its mean dF/F value). This was done to avoid issues with averaging if the animal was stationary. For each trial in the VR task, the distance aligned dLight dF/F signal during the "ramp window" of 20 to 57 cm from the start of the virtual hallway was fit with linear regression to obtain a per-trial slope. These per-trial slopes were then averaged for each day separately (Fig 3k-l) or for the last three days in each condition (Fig 3m) for subsequent statistical analysis. To visualize the group averaged distance aligned dF/F trace (Fig 3j), the mean dF/F was calculated for every 1 cm after rounding all distance values to the nearest integer.

Simulations. We previously proposed a learning model called Adjusted Net Contingency of Causal Relation (ANCCR)(20), which postulates that animals retrospectively search for causes (e.g., cues) when they receive a meaningful event (e.g., reward). ANCCR measures this retrospective association, which we call predecessor representation contingency (PRC), by comparing the strength of memory traces for a cue at rewards ($M_{\leftarrow cr}$; Equation 1) to the baseline level of memory traces for the same cue updated continuously ($M_{\leftarrow c-}$; Equation 2).

$$M_{\leftarrow cr} \equiv M_{\leftarrow cr} + \alpha[E_{\leftarrow cr} - M_{\leftarrow cr}] \tag{1}$$

$$M_{\leftarrow c-} \equiv M_{\leftarrow c-} + \alpha_0 [E_{\leftarrow c-} - M_{\leftarrow c-}] \qquad (2)$$

$$PRC_{\leftarrow cr} \equiv M_{\leftarrow cr} - M_{\leftarrow c-} \qquad (3)$$

α and α_0 are learning rates and the baseline samples are updated every dt seconds. $E_{\leftarrow ci}$ represents eligibility trace of cue (c) at the time of event i and $E_{\leftarrow c-}$ represents eligibility trace of cue (c) at baseline samples updated continuously every dt seconds. The eligibility trace (E) decays exponentially over time depending on decay parameter T (Equation 4).

$$E_{\leftarrow i}(t) = \sum_{t_i \leq t} e^{-\frac{t-t_i}{T}} \qquad (4)$$

where $t_i \leq t$ denotes the moments of past occurrences of event i. In Supplementary Note 1, we derived a simple rule for the setting of T based on event rates. For the tasks considered here, this rule translated to a constant multiplied by IRI. We have shown in a revised version of a previous study[20] that $\alpha = 1 - (1 - \alpha_0)^{\frac{IRI}{dt}}$ during initial learning. To mimic the dynamic tone condition, we simulated the occurrence of 8 different cues in a sequence with a 1 s interval between each cue. We used 1 s intervals between cues because real animals are unlikely to detect the small change in frequency occurring every 200ms in the dynamic tone, and we assumed that a frequency change of 400 Hz in 1 s was noticeable to the animals. We included the offset of the last cue as an additional cue. This is based on observation of animal behavior, which showed a sharp rise in anticipatory licking following the offset of the last cue (Fig 1f-g). Inter-trial interval was matched to the actual experimental conditions, averaging 2 s for the short dynamic condition and 49 s for long dynamic condition, with an additional 6 s fixed consummatory period. This resulted in 17 s IRI for short dynamic condition and 64 s IRI for long dynamic condition on average. 1000 trials were simulated for each condition, and the last 100 trials were used for analysis. Following parameters were used for simulation: w=0.5, b_{cues}=0, b_{reward}=0.5, threshold=0.2, T=0.2 IRI, $\alpha_0 = 5 \times 10^{-3}$, $\alpha_R = 1$, dt=0.2 s.

Statistics. All statistical tests were run on Python 3.11 using the scipy (version 1.10) package. Full details related to statistical tests are included in Supplementary Table 1. Data presented in figures with error bars represent mean ± SEM. Significance was determined using 0.05 for α. *p < 0.05, **p < 0.01, ***p < 0.001, ns p > 0.05.

Supplementary Notes

Note 1: Setting of eligibility trace time constant. It is intuitively clear that the eligibility trace time constant T needs to be set to match the timescales operating in the environment. This is because if the eligibility trace decays too quickly, there will be no memory of past events, and if it decays too slowly, it will take a long time to correctly learn event rates in the environment. Further, the asymptotic value of the baseline memory trace of event x, $M_{\leftarrow x-}$ for an event train at a constant rate λ_x with average period t_x is $T/t_x = T\lambda_x$. This means that the neural representation of $M_{\leftarrow x-}$ will need to be very high if T is very high and very low if T is very low. Since every known neural encoding scheme is non-linear at its limits with a floor and ceiling effect (e.g., firing rates can't be below zero or be infinitely high), the limited neural resource in the linear regime should be used appropriately for efficient coding. A linear regime of operation for $M_{\leftarrow x-}$ is especially important in ANCCR since the estimation of the successor representation by Bayes' rule depends on the ratio of $M_{\leftarrow x-}$ for different event types. Such a ratio will be highly biased if the neural representation of $M_{\leftarrow x-}$ is in its non-linear range. Assuming without loss of generality that the optimal value of $M_{\leftarrow x-}$ is M_{opt} for efficient linear coding, we can define a simple optimality criterion for the eligibility trace time constant T. Specifically, we postulate that the net sum of squared deviations of $M_{\leftarrow x-}$ from M_{opt} for all event types should be minimized at the optimal T. The net sum of squared deviations, denoted by SS, can be written as

$$SS = \sum_x (M_{\leftarrow x-} - M_{opt})^2 = \sum_x (T\lambda_x - M_{opt})^2 \tag{5}$$

Where the second equality assumes asymptotic values of $M_{\leftarrow x-}$. The minimum of SS with respect to T will occur when $\frac{\partial SS}{\partial T} = 0$. It is easy to show that this means that the optimal T is:

$$T_{opt} = M_{opt} \frac{\sum_x \lambda_x}{\sum_x \lambda_x^2} \tag{6}$$

For typical cue-reward experiments with each cue predicting reward at 100% probability, $\lambda_{cue} = \lambda_{reward} = \frac{1}{IRI}$. Substituting into the above equation, we get:

$$T_{opt} = M_{opt} . IRI \tag{7}$$

Thus, in typical experiments with 100% reward probability, the eligibility trace time constant should be proportional to the IRI or the total trial duration, which is determined by the ITI—the experimental proxy that we manipulate. Please do note, however, that the above relationship is not strictly controlled by the ITI, but by the frequency of repeating events in the environment (i.e., environmental timescale).

Note 2: Higher cue-offset induced anticipatory licking with short ITI. We observed empirically that the animals showed higher anticipatory licking following cue offset (i.e., 8 seconds after cue onset) during the short ITI condition compared to the long ITI condition (Fig 1f) (though this is only weakly significant). We believe that this simply reflects the fact that the cue onset is relatively much farther to reward delivery compared to the inter-cue interval during the short ITI condition compared to the long ITI condition (ratio of 9s to 9+8s in short ITI vs 9s to 9+55s in the long ITI). Therefore, in the short ITI condition, the cue offset provides a stronger signal indicating relative proximity to reward.

Note 3: The implications of assuming that internal states may serve the role of external cues in ANCCR. Some readers will note that we have previously argued against the assumption of internal states serving the role of externally signaled events in learning theories(46). It may therefore seem that our speculation that internal states can serve this role during timing tasks is problematic. However, there is a critical difference between our earlier position and the current speculation. Our earlier position was that assuming fixed internal states that pre-exist and provide a scaffold for learning, such as in temporal difference learning, is problematic. This is because these pre-existing states would need to already incorporate information that can only be acquired during the course of learning. Unlike this position, here we are merely speculating that after learning, an internal progression of states can serve the function of externally signaled events. Similarly, we have previously postulated that such an internal state exists during omission of a predicted reward, but only after learning of the cue-reward association.

Note 4: Some discrepancies between ANCCR simulations and experiments. We performed the ANCCR simulations not to explicitly fit the experiments, but to motivate them. Accordingly, there are many details of the experimental conditions that we did not include in the simulations. First, animals were trained initially using a long (Pavlovian) or medium ITI (VR), thereby establishing that the cue onset is a meaningful event before switching to the short ITI. Second, animals are unlikely to discriminate each change in tone frequency in the dynamic tone (80 Hz every 200 ms). Thus, we simplified the simulation and used a 1 s interval between sensory cues under the assumption that 400 Hz would be discriminable. The potential sensory noise in detection of frequency changes was not modeled in the simulation. Third, we did not explicitly model potential trial-by-trial changes in eligibility trace time constant, sensory noise, or internal threshold. Fourth, we did not simulate any biophysical mechanisms controlling dopamine release, or sensor dynamics. Thus, we did not expect to capture all experimental observations
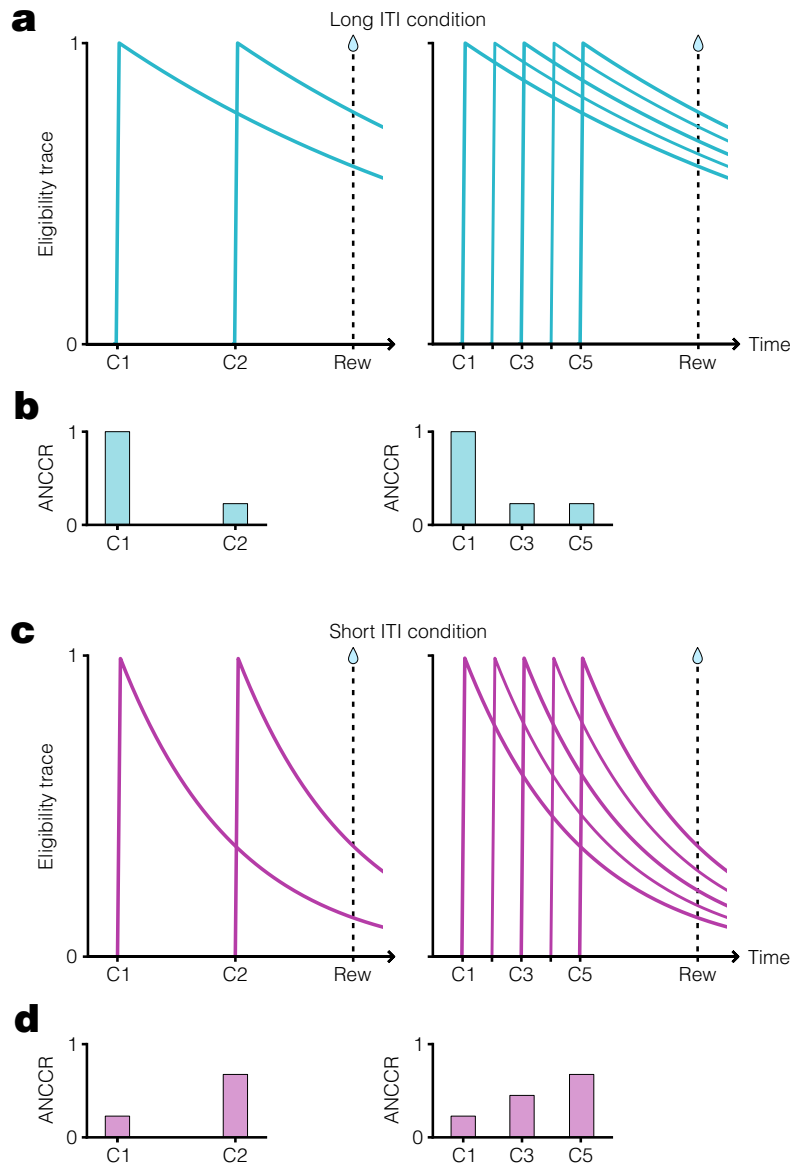
in the motivating simulation. One particular discrepancy is worth noting: the cue onset response in the short ITI condition is small but positive in the experiment but negative in ANCCR. This may potentially reflect the fact that the cue onset was already learned to be meaningful prior to the short ITI experiment.

Supplementary Table 1: Statistical Details.

Figure	Description	Test	Statistic	p value	Sample size
1g	Anticipatory lick rate across ITI (long, short) and tone (fixed, dynamic)	Two-way ANOVA	ITI: $F_{(1)} = 9.30$ Tone: $F_{(1)} = 0.30$ ITI x Tone: $F_{(1)} = 0.029$	ITI: **p = 0.00457 Tone: p = 0.586 ITI x Tone: p = 0.865	n = 9 mice
1j	Cue onset peak dLight between conditions (LD, SD)	Paired t-test	$t_{(8)} = 6.31$	***p = 2.31×10^{-4}	n = 9 mice
1l	Slope between days (LD condition last day, SD condition first day)	One-sided (LD < SD) paired t-test	$t_{(8)} = -2.07$	*p = 0.0363	n = 9 mice
1l	Slope between days (SD condition last day, SF condition first day)	One-sided (SD > SF) paired t-test	$t_{(8)} = 2.35$	*p = 0.0233	n = 9 mice
1m	Slope across conditions (LF, LD, SD, SF)	One-way ANOVA	$F_{(3)} = 8.89$	***p = 1.98×10^{-4}	n = 9 mice
1m	Slope across conditions (LF, LD, SD, SF)	Tukey HSD test for multiple comparison of means	$q = 3.83$	LD vs LF: p = 0.762 LD vs SD: **p = 0.00266 LD vs SF: p = 0.952 LF vs SD: ***p = 1.70×10^{-4} LF vs SF: p = 0.445 SD vs SF: *p = 0.0107	n = 9 mice
2b	Trial slope regression β given previous ITI (SD condition only)	One-sided (< 0) one sample t-test	$t_{(8)} = -2.17$	*p = 0.0308	n = 9 mice
2c	Trial slope given previous ITI (SD condition only)	Linear regression	$t_{(2671)} = -4.13$ $R^2 = 0.00634$	***p = 3.77×10^{-5}	n = 2672 trials
3e	Change in velocity at trial onset (long ITI condition only)	One-sided (> 0) one sample t-test	$t_{(8)} = 6.40$	***p = 1.05×10^{-4}	n = 9 mice
3e	Change in velocity at trial onset (short ITI condition only)	One-sided (> 0) one sample t-test	$t_{(8)} = 7.93$	***p = 2.33×10^{-5}	n = 9 mice
3e	Change in velocity at trial onset between conditions (long, short)	Paired t-test	$t_{(8)} = 4.25$	**p = 0.00281	n = 9 mice
3g	Pre-reward velocity between conditions (long, short)	Paired t-test	$t_{(8)} = 0.71$	p = 0.497	n = 9 mice
3i	Cue onset peak dLight between conditions (long, short)	Paired t-test	$t_{(8)} = 7.59$	***p = 6.34×10^{-5}	n = 9 mice
3l	Session slope given session IRI (both long and short ITI conditions)	Linear regression	$t_{(53)} = -2.61$ $R^2 = 0.116$	*p = 0.0118	n = 54 sessions
3m	Slope between conditions (long, short)	One-sided (long < short) paired t-test	$t_{(8)} = -2.09$	*p = 0.0349	n = 9 mice

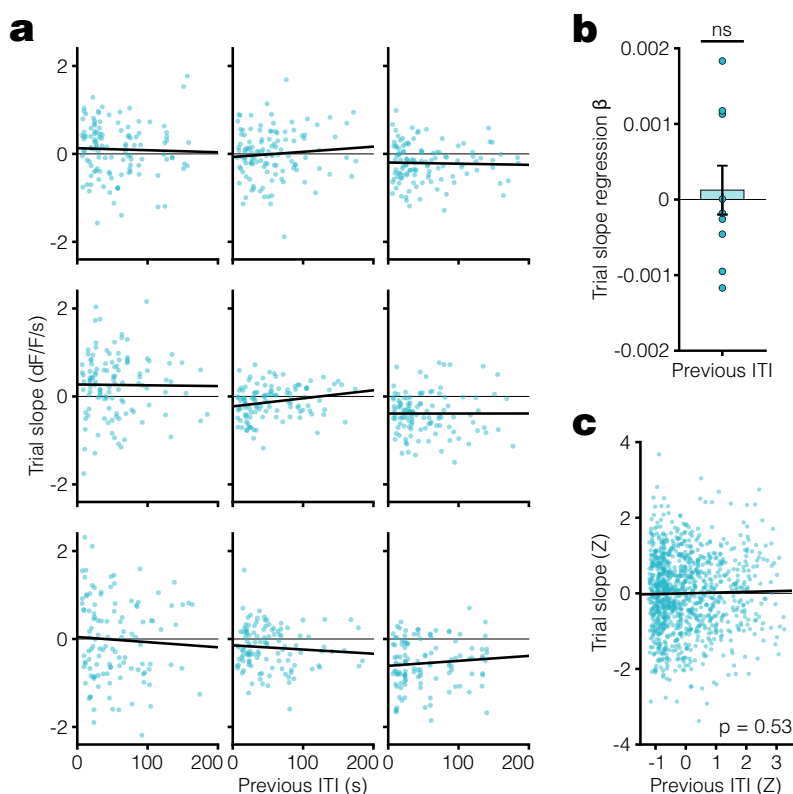| Figure	Description	Test	Statistic	p value	Sample size
Ext 2d	Lick rate during ramp window across conditions (LF, LD, SD, SF)	One-way ANOVA	$F(3) = 0.81$	$p = 0.498$	n = 9 mice
Ext 3b	Trial slope regression β given previous ITI (LD condition only)	One-sided (< 0) one sample t-test	$t(8) = 0.36$	$p = 0.637$	n = 9 mice
Ext 3c	Trial slope given previous ITI (LD condition only)	Linear regression	$t(1050) = 0.64$ $R^2 = 3.85 \times 10^{-4}$	$p = 0.525$	n = 1051 trials
Ext 4c	Trial duration between conditions (long, short)	Paired t-test	$t(8) = 1.02$	$p = 0.336$	n = 9 mice
Ext 4e	Anticipatory lick rate (long ITI condition only)	One-sided (> 0) one sample t-test	$t(8) = 2.89$	$*p = 0.0101$	n = 9 mice
Ext 4e	Anticipatory lick rate (short ITI condition only)	One-sided (> 0) one sample t-test	$t(8) = 4.38$	$**p = 0.00118$	n = 9 mice
Ext 4e	Anticipatory lick rate between conditions (long, short)	Paired t-test	$t(8) = 1.08$	$p = 0.311$	n = 9 mice
Ext 5b	Trial slope regression β given previous IRI (short ITI condition only)	One-sided (< 0) one sample t-test	$t(8) = -0.48$	$p = 0.321$	n = 9 mice
Ext 5c	Trial slope given previous IRI (short ITI condition only)	Linear regression	$t(1301) = -2.11$ $R^2 = 0.00339$	$*p = 0.0355$	n = 1302 trials

Table 1. Statistical Details.

Floeder, Jeong, Mohebi, Namboodiri | Mesolimbic dopamine ramps reflect environmental timescales

Extended Data Figure 1. Dependence of ANCCR on eligibility trace time constant. a. Schematic showing exponential decay of cue eligibility traces for a two-cue sequential conditioning task (left) and a multi-cue conditioning task (right) with a long inter-trial interval (ITI). In this case, a long ITI results in a proportionally large eligibility trace time constant, T, producing slow eligibility trace decay (Supplementary Note 1). Reward delivery time indicated by vertical dashed line. **b**. Schematized ANCCR magnitudes (arbitrary units) for cues in the two-cue (left) and multi-cue (right) conditioning tasks with a long ITI. Since the eligibility trace for the first cue is still high at reward time, there is a large ANCCR at this cue. The remaining cues are preceded consistently by earlier cues associated with the reward, thereby reducing their ANCCR. **c**. Same conditioning task trial structure as in a, but with a short ITI and smaller T, producing rapid eligibility trace decay. **d**. Schematized ANCCR magnitudes for cues in both conditioning tasks with a short ITI. Since the eligibility trace for the first cue is low at reward time, there is a small ANCCR at this cue. Though the remaining cues are preceded consistently by earlier cues associated with the reward, the eligibility traces of these earlier cues decay quickly, thereby resulting in a higher ANCCR for the later cues.
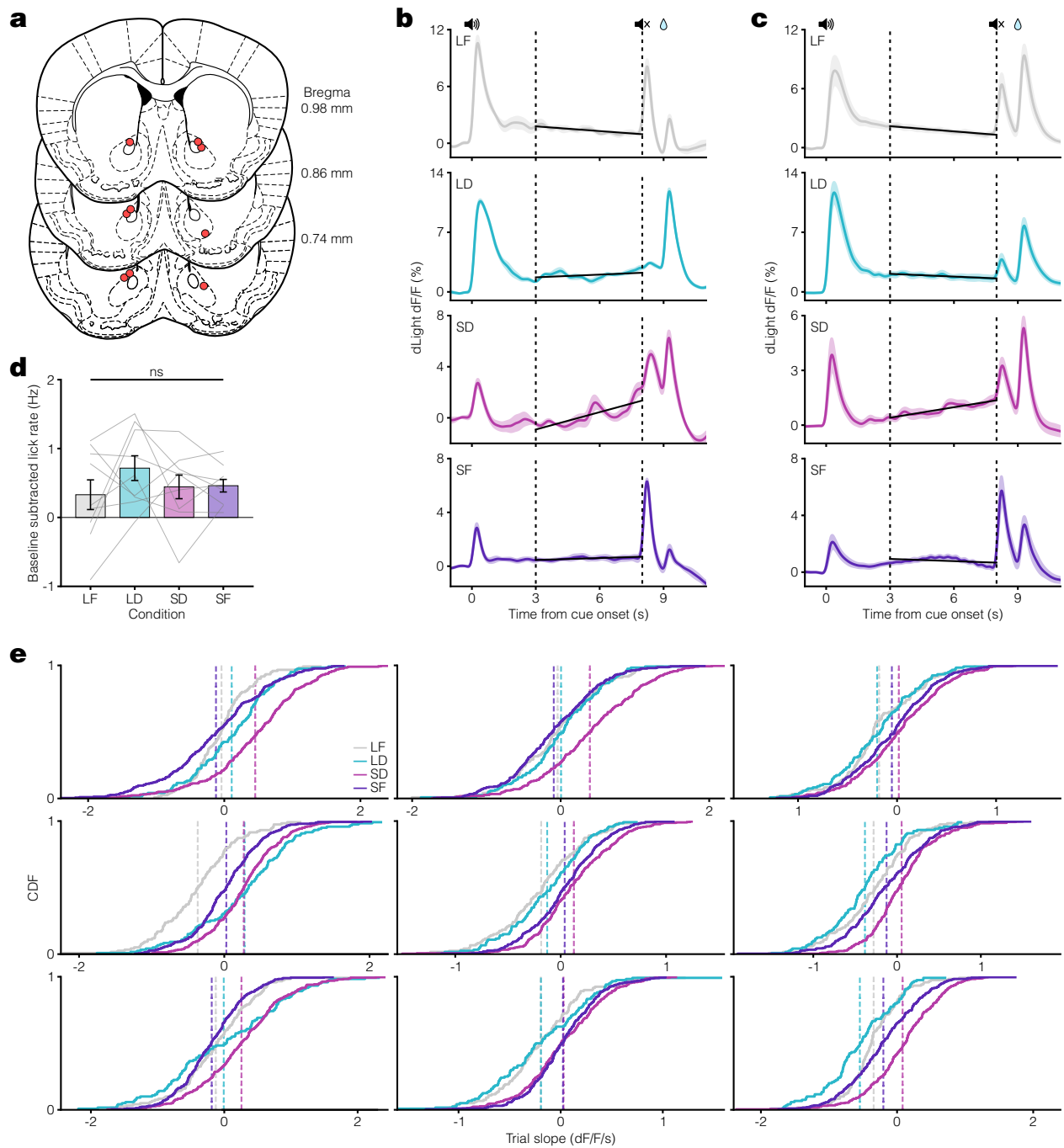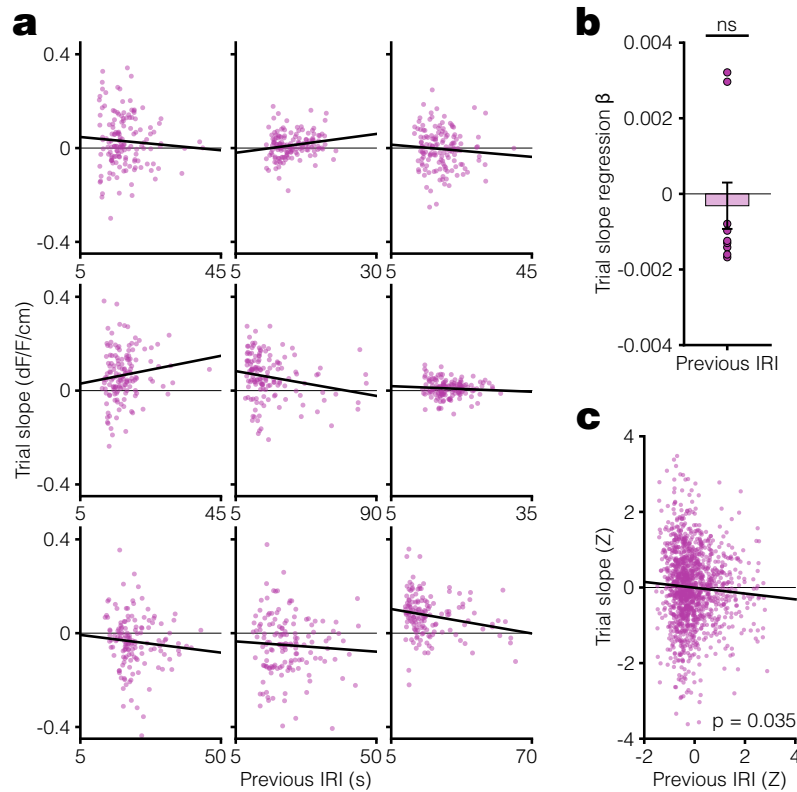
Extended Data Figure 2. Pavlovian conditioning histology and responses. a. Mouse coronal brain sections showing reconstructed locations of optic fiber tips (red circles) in NAcC for Pavlovian conditioning task. **b**. Example average dLight traces for the last three days of all conditions. Vertical dashed lines at 3 and 8 s represent the ramp window period. Black lines display the linear regression fit during this period. **c**. Same as in b but for the average dLight traces across all animals. **d**. Comparison of average baseline subtracted lick rate during the ramp window across all conditions (one-way ANOVA: F(3) = 0.81, p = 0.50). **e**. Individual plots for each mouse displaying the cumulative distribution of per-trial slopes for the last three days in all conditions. Vertical dashed lines indicate the average trial slope for LF (grey), LD (teal), SD (pink), and SF (purple) conditions.

Floeder, Jeong, Mohebi, Namboodiri | Mesolimbic dopamine ramps reflect environmental timescales

Extended Data Figure 3. Trial-by-trial correlations for long ITI/dynamic tone condition. a. Scatter plots showing the relationship between dopamine response slope within a trial and previous ITI for all trials in the last 3 days of LD condition. Each animal plotted individually with linear regression fit (black line). **b**. Linear regression β coefficients for previous ITI predicting trial slope (one-sided [< 0] one sample t-test: t(8) = 0.36, p = 0.64). **c**. Scatter plot of Z-scored trial slope vs. previous ITI pooled across mice for all trials in the last 3 days of LD condition (linear regression: t(1050) = 0.64, R^2 = 3.9 $\times 10^{-4}$, p = 0.53).
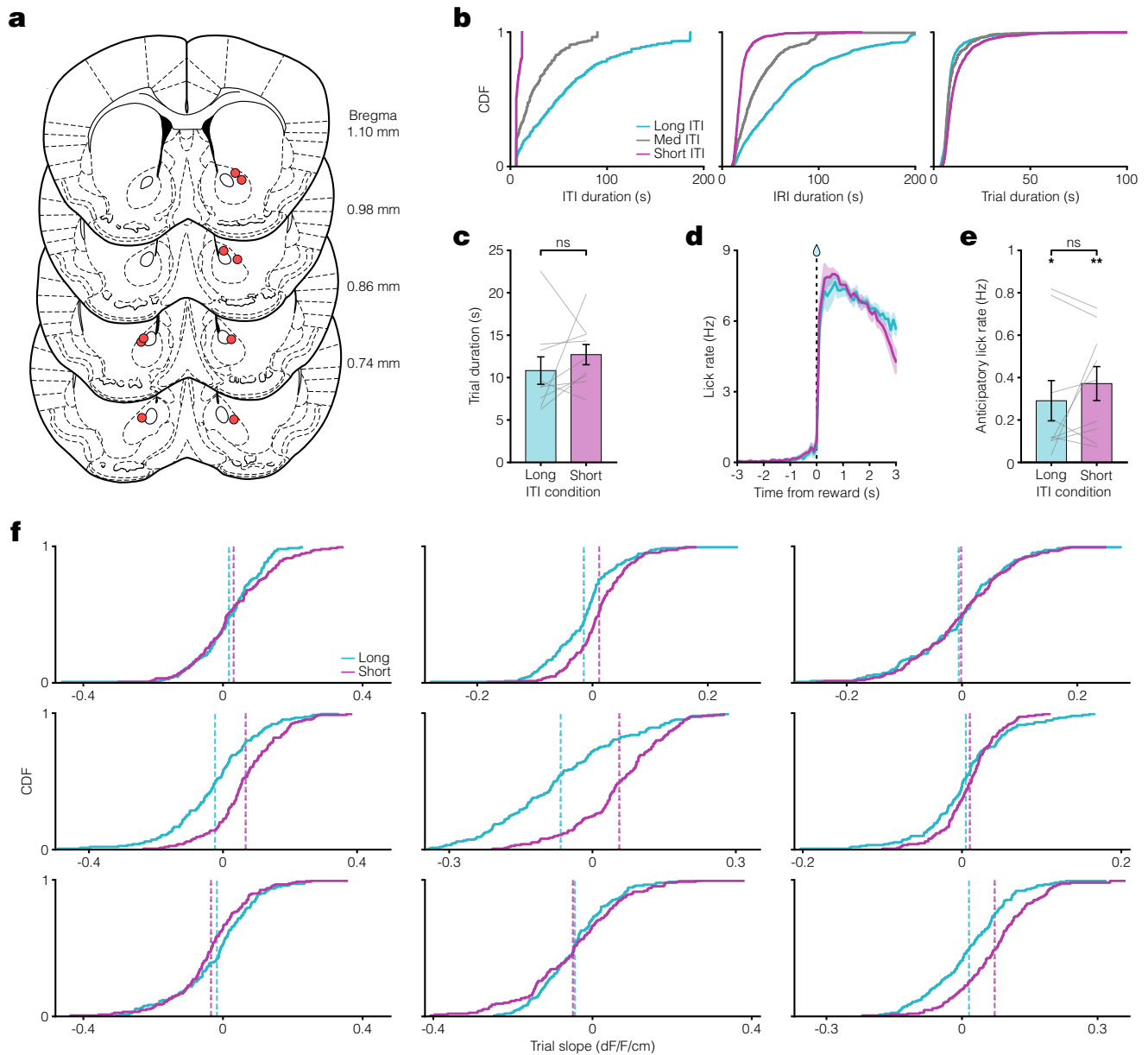
Extended Data Figure 4. VR task histology and responses. a. Mouse coronal brain sections showing reconstructed locations of optic fiber tips (red circles) in NAcC for VR navigation task. **b**. Left, CDF of ITI duration for long (teal), medium (grey), and short (pink) ITI conditions. Middle, CDF plot of inter-reward interval (IRI) durations for each condition. Right, CDF plot of trial durations for each condition. **c**. Comparison of average trial duration for long and short ITI conditions (paired t-test: t(8) = 1.0, p = 0.34). **d**. Lick rate PSTH aligned to reward delivery indicates minimal anticipatory licking behavior. **e**. Quantification of average anticipatory lick rate 1 s before reward delivery. Bottom asterisks indicate a positive anticipatory lick rate for both ITI conditions (one-sided [> 0] one sample t-test: long ITI t(8) = 2.9, *p = 0.010; short ITI t(8) = 4.4, **p = 0.0012), though there was no significant difference between conditions (paired t-test: t(8) = 1.1, p = 0.31) **f**. CDF plots for each mouse separately showing the distribution of per-trial slopes for the last three days in both conditions. Vertical dashed lines indicate the average trial slope for long (teal) and short (pink) ITI conditions.

Floeder, Jeong, Mohebi, Namboodiri | Mesolimbic dopamine ramps reflect environmental timescales

Extended Data Figure 5. Trial-by-trial correlation of dopamine response slope vs previous inter-reward interval (IRI) in the VR task. a. Scatter plot of dopamine response slope on a trial and the previous IRI for individual animals in the VR task during the short ITI condition. Here, we are measuring the environmental timescale using IRI instead of ITI because the trial duration in this task (see Supplementary Note 1) depends on the running speed of the animals, which varies trial to trial. Thus, IRI measures the net time interval between successive trial onsets. In the Pavlovian conditioning task, IRI and ITI differ by a constant since the trial duration is fixed. **b**. Linear regression β coefficients for previous IRI vs trial slope calculated per animal (one-sided [< 0] one sample t-test: t(8) = -0.48, p = 0.32). c. Scatter plot of Z-scored trial slope vs. previous IRI pooled across mice for all trials in the last 3 days of the Short ITI condition (linear regression: t(1301) = -2.11, R^2 = 0.0034, *p = 0.035).